

# INVESTIGATING THE PERFORMANCE OF ISOLATION SYSTEMS IN IMPROVING THE SEISMIC BEHAVIOR OF URBAN BRIDGES. A CASE STUDY ON THE HESARAK BRIDGE

**Ali Akbar Edalati<sup>1,2</sup> and Hossein Tahghighi<sup>3\*</sup>**

**ABSTRACT.** This paper investigates the influence of isolation systems on the seismic behavior of urban reinforce concrete bridge. The performance of the Hesarak Bridge constructed in Karaj city, Iran with two isolation systems; i.e. the existing elastomeric rubber bearing (ERB) and a proposed lead rubber bearing (LRB) is discussed. The numerical model was implemented in the well-known FEM software CSIBridge. The isolated bridge has been analyzed using nonlinear time history analysis method with seven pairs of earthquake records and the results are compared for the two isolation systems. The LRB isolators are shown to have superior seismic performance in comparison with the existing ERB systems based on the response evaluation including force on the isolator, pier base shear, deck acceleration, bending moment, pier displacement, and energy dissipation.

*Keywords:* RC bridge, Seismic response, LRB, ERB, Time history analysis

## 1. INTRODUCTION

The bridges are the main parts of transportation that must be fitted to earthquake hazards. Thus, the capacity of the bridges should be higher than its demand. By increasing the ground acceleration, the force on the bridge increases and the bridge's capacity should be increased, which is to some extent acceptable and rational. In such cases, design codes allow the use of ductility to increase capacity.

<sup>1</sup>MSc in Structural Engineering, University of Kashan, Kashan, Iran, Post Code: 8731753153, Email: [aliakbar.edalati1@gmail.com](mailto:aliakbar.edalati1@gmail.com) (Ali Akbar Edalati) ORCID code: <https://orcid.org/0000-0002-4225-2965>

<sup>2</sup>Structural Engineer, Civil Organization, Municipality of Karaj, Karaj, Iran, Post Code: 3134851889.

<sup>3</sup>Assistant Prof., PhD, PE, Civil Eng. Dept., University of Kashan, Kashan, Iran, Post Code: 8731753153 ORCID code: <https://orcid.org/0000-0001-6091-8815>

\*Corresponding author Tel.: +98 31 55912430; Fax: +98 31 55912424; Postal code: 8731753153.  
E-mail: [tahghighi@kashanu.ac.ir](mailto:tahghighi@kashanu.ac.ir) (Hossein Tahghighi).

Isolation of the structure is typically used to support the deck on the piers and the abutments and reduce the effects of seismic loads and thermal effects on bridges [1]. Since 1970, a range of isolation devices has been developed in aseismic design structures [2]. The LRB is most commonly used base isolation system. The bearing is very stiff and strong in the vertical direction, but flexible in the horizontal direction. Roy and Dash [3] observed that the response parameters significantly reduce for a multi-span bridge seismically isolated by LRB over non-isolation bearing.

The LRB rubber isolators have a bi-linear behavior that reduces the stiffness of the second part of the curve by yielding the lead. In other words, it is softened and produces an optimal performance against severe and slight seismic loads [4, 5]. The lead core causes energy loss and increases the structure damping, and the steel layers increase vertical bearing capacity. LRB isolators in combination with elastomeric bearings distribute earthquake forces between abutments and piers [6]. Unlike the LRB isolators, the ERBs are not able to properly distribute earthquake forces between the piers and abutments during an earthquake ground motion, and in some cases do not work as isolators at all [7]. The LRB are multilayered, laminated elastomeric bearings that have one or more circular holes. Lead plugs are inserted into these holes to add damping to the isolation system [8]. The occurrence of tensile forces in isolation bearings has been reported in many reconnaissance surveys such as those following the 2011 Tohoku earthquake and also in experimental shaking-table tests on isolated structures [9]. Mendez et al. [10] demonstrated in full-scale experiments the proper function of LRB isolators in energy losses during cyclic loads and effective operation against displacements. The LRB isolator has been shown to function properly under the near-and far-fault zone earthquake motions [11]. The natural period of the structure and the isolation coefficient of friction are the most critical parameters that control the isolator function [12].

When an isolated bridge is subjected to an earthquake, deformation occurs in the isolators instead of the substructure elements. This greatly reduces the forces transmitted from the superstructure to the substructure. Over the past 20 years, more than 200 bridges in the United States have been designed or renovated using seismic isolation, and more than a thousand bridges around the world have now been used with this affordable technology for seismic protection [13]. Seismic isolation with ERB has been used extensively in contemporary bridge engineering in Iran as a means of mitigating the effect of earthquake loads [14]. In this study, the application of LRB isolation system has been investigated to evaluate the seismic responses of the Hesarak Bridge including vibration period, base shear, lateral

displacement and bending moment of the piers, deck acceleration, damping and energy dissipation in comparison to the influence of existing ERB isolation system. Thus, first, the isolation systems and their seismic performances are introduced. Then, a comprehensive parametric study is carried out to investigate the effectiveness of LRB over ERB isolation systems for the multi-span urban bridge using nonlinear modal time history analysis method.

## 2. BRIDGE DESCRIPTION

The Hesarak reinforce concrete bridge is located on the Karaj-Qazvin freeway along the Shahid Beheshti Blvd. in the city of Karaj, Iran. Fig. 1 shows the aerial photo of the bridge. It has a concrete deck and concrete walls of piers as depicted in Fig. 2. Deck section is single-cell, pre-fabricated and pre-stressed. Figs. 3 through 5 show deck cross-section, abutment details, pier section, and longitudinal profile of the bridge, respectively [16]. The width of the bridge is 14.2 m and the length of the spans is variable. The bridge has wall middle columns, seven spans and a total length of 302.4 m, a width of 14.2 m, the longest span is 58.25 m and the shortest span is 25.45 m. Table 1 shows the detailed information of the bridge.

The main components of the deck are the top slab, the cantilever segment, the web, and the bottom slab. The tendons used in the bridge deck are of 270 GR-270 types with the ultimate resistance of 18700 kg/cm<sup>2</sup>. The type of cables is strand and they are seven wires, with a nominal diameter of 1.5 cm. The compressive strength of concrete used in the deck is considered to be 300 kg/cm<sup>2</sup>. While, concrete used in piers, abutment, cap, and piles has a compressive strength of 250 kg/cm<sup>2</sup>. The rebars used in the bridge are AIII grade with a yield strength of 4000 kg/cm<sup>2</sup> [16]. According to the field test experiments, the site soil type II ( $375 < V_s < 750$  m/sec) is considered based on the Standard No. 2800 [17]. Also, the coefficient of design acceleration  $A=0.35$ , and the period values  $T_0$  and  $T_s$  are considered to be 0.1 and 0.5 sec, respectively. The deep foundation located below the piers consists of a pile head 8.5 m by 5.5 m and a thickness of 1.5 m. Piles are single with a rectangular cross-section measuring from 0.8 m to 3.6 m and a height of 18 m.



Figure 1. Aerial photo of the Hesarak Bridge [15].



Figure 2. General view of the Hesarak Bridge.

Seismotectonic studies indicate that the Hesarak Bridge is located in the site with high seismic activity [16]. The north Tehran fault is the nearest fault to the site, which is about 4 km away from the bridge. Note that near-fault motions are considerably affected by the forward rupture directivity [18]. However, the detailed seismic assessment of the bridge due to the effects of near-fault ground motion can be an interesting issue for further future researches. Furthermore, the effects of soil-structure interaction are neglected in this study. In other words, it is assumed that the foundation of the bridge is fixed against all the movements. It is worth mentioning that Tahghighi and Rabiee [19] concluded that ignoring base flexibility may over or under predict seismic response of the structure depends mainly on the soil-structure relative rigidity. Therefore, the soil-pile-bridge interaction should be considered as a further study on the seismic response of the bridge. In the following, the bridge's seismic behavior has been evaluated using the LRB isolators as of the proposed isolator system and compared with the current status of the bridge, which includes ERB isolators.

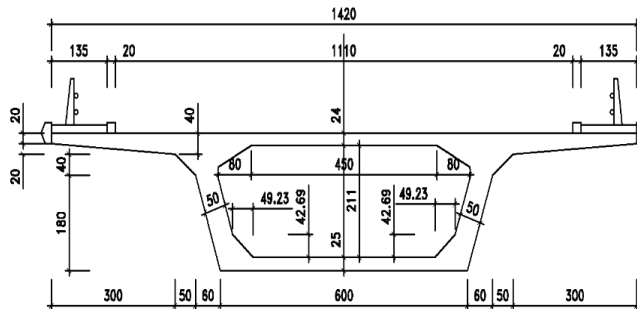


Figure 3. Cross-section through the deck of Hesarak Bridge (unit in cm) [16].

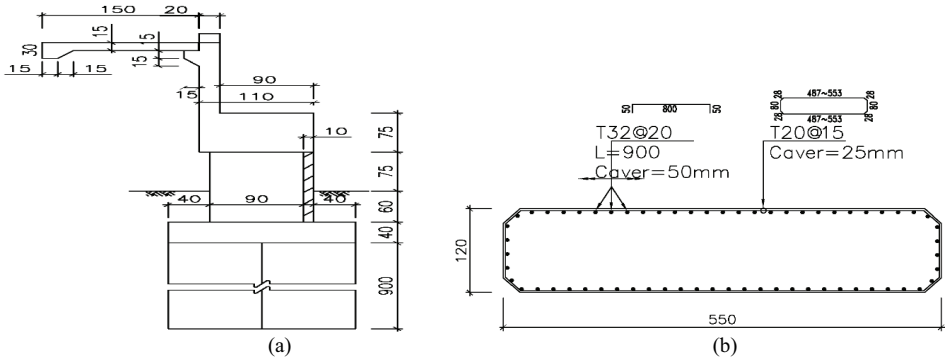


Figure 4. Details of the Hesarak Bridge (unit in cm): a) Abutment, and b) Pier section [16].

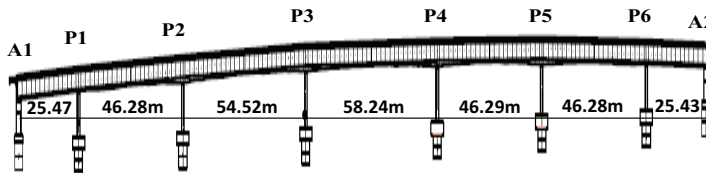


Figure 5. Longitudinal profile of the bridge [16].

Table 1. Specifications of the bridge

Bridge specifications	Quantity
Bridge length (m)	302.4
Bridge width (m)	14.2
Piers height* (m)	5.28, 5.79, 6.64, 6.61, 6.15, 5.52
Number of spans	7
Span length** (m)	25.47, 46.28, 54.52, 58.24, 46.29, 46.28, 25.43
Piers width (m)	5.5

\*: The pier's height is from the left to the right side of the bridge.

\*\* : The length of spans is from the left to the right side of the bridge.

### 3. FINITE ELEMENT MODEL

In order to investigate the isolated bridge response, the three-dimensional numerical modeling was performed utilizing the finite element software CSIBridge [20]. The 3D model of the bridge is shown in Fig. 6. According to the design codes, it is assumed that the elements of the superstructure and the substructure remain elastic. Therefore, the substructure elements like piers and elements of the superstructure, namely the deck, are modeled using a frame element that has linear behavior. The

nonlinear link element is used to model the isolator bearing, which during a response history analysis is capable of providing nonlinear behavior. The columns at the bottom end are based on a rigid foundation and the interaction of soil and structure are neglected.

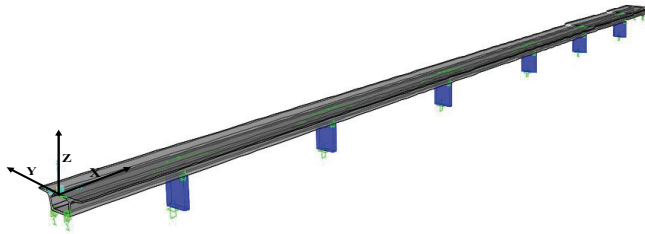


Figure 6. 3D finite element model of the bridge.

### 3.1. BRIDGE DECK

As shown in Fig. 3, the deck section of the bridge is a pre-stressed box girder concrete with a single-cell and width of 14.2 m. The bridge deck was modeled with a frame element that has linear behavior.

### 3.2. LATERAL AND MIDDLE PIERS

Lateral piers (abutments) are reinforced wall, which interacts with the soil around. Fig. 4a illustrates the detail of the abutments of the Hesarak Bridge. The abutments are assumed to be rigid due wing wall, and the bottom end of the abutments is assumed to be fixed. The middle piers of the RC type wall with a dimension of 1.2 m by 5.5 m with a variable height of 5 to 7 m are considered following Fig. 4b and it is exerted to the numerical model as a frame element. As mentioned before, the connection of the bottom ends of the middle piers to the foundation is fixed.

### 3.3. ERB ISOLATOR

The ERB isolator is a common type of supports in concrete bridges. These supports transmit the horizontal force by means of friction, and their behavior depends very much on the initial stiffness. ERB isolators are modeled using a linear link element. In finite element modeling, it is necessary to determine the vertical and shear stiffness of the isolator. The shear stiffness,  $k_H$ , and axial stiffness,  $k_V$ , of the ERB isolators are defined by Equations (1) and (2), respectively.

$$K_H = \frac{GA}{T_r} \tag{1}$$

$$K_V = \frac{E_c A}{T_r} \tag{2}$$

where  $G$  is the shear modulus of the elastomer,  $A$  is the cross-sectional area of the bearing,  $T_r$  is the total thickness of rubber layers, and  $E_c$  is the instantaneous compression modulus of the elastomer. The value of  $E_c$  is obtained from Eq. (3) for the rectangular isolators.  $S$  is the shape factor which is defined following the AASHTO guide specifications for isolation design [21] (Eq. (4)). In Eq. (4),  $B$  and  $L$  are width and length of the ERB, respectively, and  $t_i$  is the thickness of one rubber layer. According to the explained procedures, the ERB specifications used in the bridge is given in Table 2.

$$E_c = 4GS^2 \tag{3}$$

$$S = \frac{BL}{2t_i(B + L)} \tag{4}$$

Table 2. ERB isolator specifications used in the bridge

	<b>ERB dimension (mm)</b>	<b><math>G</math> (kg/cm<sup>2</sup>)</b>	<b><math>E_c</math> (kg/cm<sup>2</sup>)</b>	<b><math>K_H</math> (ton/m)</b>	<b><math>K_V</math> (ton/m)</b>
<b>Lateral piers</b>	900×900×59	10	3550	1373	487373
<b>Middle piers</b>	900×900×95	10	3550	853	302684

### 3.4. LRB ISOLATOR

The isolation design of a bridge with lead rubber bearings primarily involves the determination of the properties of the isolators themselves. Fig. 7 shows the components of an LRB system. Where  $d$  and  $H$  are the diameter and the total height of isolator, respectively.  $d_l$  and  $h_l$  are the diameter and the height of lead core, respectively. Elastomeric LRB is considered as an ideal bi-linear hysteresis model with nonlinear characteristics in shear freedom degrees and linear properties in other degrees of freedom. In order to model the isolator, the spring element (Link) is used. The shear and axial mechanical behavior of the LRB isolator is shown in Fig. 8. The nonlinear model is based on the hysteretic behavior provided by Park et al. [22]. According to this method, the parameters required for an LRB isolator are the initial elastic stiffness ( $K_{el}$ ), yield strength ( $F_y$ ), post-yield stiffness ( $K_d$ ), and effective stiffness ( $K_{eff}$ ). Table 3 presents the material properties of rubber used in isolator design.  $G_r$  is the shear modulus of rubber,  $K$  is the bulk modulus of rubber, and  $k'$  is the material constant for rubber.

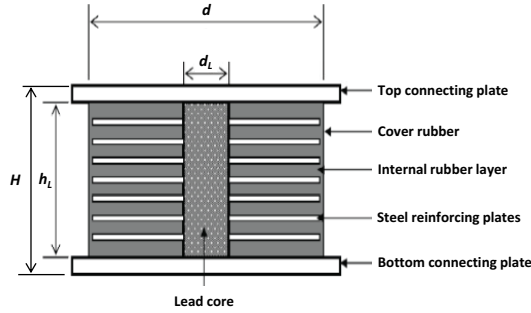


Figure 7. LRB isolator system (after [13]).

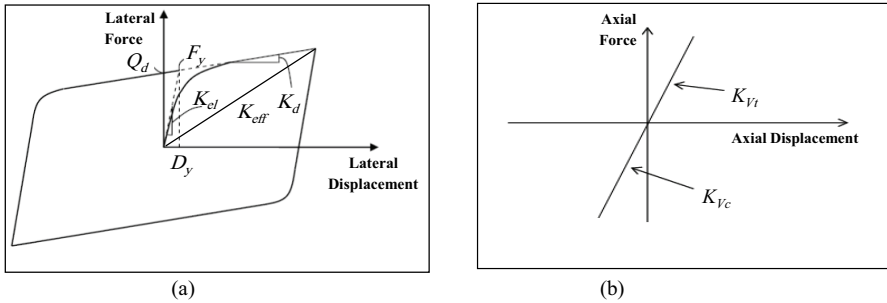


Figure 8. Force-displacement model for LRB: a) Shear behavior, and b) Axial behavior.

Table 3. Material properties of rubber used in LRB design

$G_r$ ( $\text{kg/cm}^2$ )	$K$ ( $\text{kg/cm}^2$ )	$K'$
6.4	20000	0.73

Following AASHTO guideline [21], the LRB has been designed for the bridge. The properties of the isolators which need to be determined to complete the design include lead core diameter, isolator diameter, thickness and number of the rubber layers, thickness and number of steel reinforcing plates. Equations (5) through (9) have been used to calculate the LRB properties.

$$D_d = \left( \frac{250AS_iT_e}{B_L} \right) \tag{5}$$

$$K_e = \frac{W}{n_{bg}} \left( \frac{4\pi^2}{T_e^2} \right) \tag{6}$$



$$Q_i = \frac{1}{2} \pi \zeta K_e D_d \tag{7}$$

$$K_d = K_r \left( 1 + 12 \frac{A_p}{A_b} \right) \tag{8}$$

$$K_{pd} = \frac{Q_d}{D_d} \tag{9}$$

Where  $D_d$  is the design displacement,  $A$  is the acceleration coefficient,  $S_i$  is the site coefficient for seismic isolation,  $T_e$  is the effective period,  $B_L$  is the damping coefficient corresponding to damping ratio ( $\zeta=30\%$ ),  $K_e$  is the required effective stiffness of the bearings,  $W$  is the weight of the bridge superstructure,  $n_b$  is the number of bearings, and  $g$  is the gravitational acceleration constant.  $Q_i$  is initial required characteristic strength (seismic resistance) of the lead core.  $K_r$  is stiffness provided by rubber,  $A_p$  is lead core area, and  $A_b$  is the bonded plan area of the bearing.  $K_{pd}$  is lead core stiffness and  $Q_d$  is characteristic strength. The design recommendation by Naeim and Kelly [5] for  $K_d/K_{el}$  is 0.1. Accordingly, Table 4 shows the detailed information of the LRB calculated for the bridge.

Table 4. LRB isolator specifications

$T_e$ (sec)	$d_L$ (mm)	$d$ (mm)	$h_L$ (mm)	$H$ (mm)	$t_i$ (mm)	$T_r$ (mm)	$D_d$ (cm)	$Q_d$ (Kg)	$K_{el}$ (Kg/m)	$F_y$ (Kg)	$K_{eff}$ (Kg/m)
2.7	200	1000	500	550	16.7	386	19.3	28260	1644577	31400	310884

#### 4. GROUND MOTION RECORDS

A database of seven recorded ground motion time histories with a wide range of intensity, duration, frequency contents and earthquake magnitudes (i.e.,  $M_w$  6.2-7.3) has been compiled from well-known studied seismic events. The ground motion records for time history analysis should, as far as possible, have characteristics similar to the probable earthquake record in the site. In other words, the design earthquake conditions must be persuaded. Table 5 lists the characteristics of interest for the selected site ground motion records [23]. In Table 5,  $R_{rup}$  is the nearest distance to the fault,  $M_w$  is earthquake magnitude,  $V_s$  is shear wave velocity, and  $PGA$  is the peak ground acceleration in the longitudinal (L), transverse (T) and vertical (V) direction. Note that each pair of motions shall be scaled such that in the period range from  $0.5T_D$  to  $1.25T_M$ , the average of the SRSS spectra from all horizontal component pairs does not fall below the corresponding ordinate of the design spectrum [24].  $T_D$  and  $T_M$  are the effective periods of the isolated bridge calculated for Design based earthquake and Maximum considered earthquake, respectively.

Table 5. Specifications of the accelerograms used in the analysis [23]

No.	Earthquake	Station	Year	$M_w$	Mechanism	$R_{rup}$ (km)	$V_s$ (m/sec)	$PGA$ (g)		
								L	T	V
1	Tabas	Dayhook	1978	7.30	Reverse	13.90	471.53	0.324	0.41	0.19
2	El Centro	El Centro Array	1940	6.95	Strike slip	6.09	213.44	0.28	0.21	0.17
3	Cape Mendocino	Petrolia	1992	7.00	Reverse	8.20	422.17	0.59	0.66	0.16
4	Northridge	Pacoima Kagel	1994	6.70	Reverse	7.20	508.08	0.301	0.43	0.17
5	Kobe	Nishi-Akashi	1995	6.90	Strike slip	7.10	609.00	0.483	0.46	0.38
6	Chi Chi	TCU084	1999	6.20	Reverse	9.30	665.20	0.139	0.06	0.05
7	San Simeon	Cambria	2003	6.50	Reverse	7.20	362.42	0.206	0.15	0.08

## 5. NUMERICAL ANALYSIS

The most suitable method of analysis consistent with the physical behavior of structures subjected to earthquake excitations is the nonlinear time history analysis. In the response history analysis, the effect of earthquake stimulation on a structure is considered more realistic than other dynamic analysis methods. If seven or more pairs of ground motions are used for the response history analysis, the average value of the response parameter of interest is permitted to be used for design. If fewer than seven pairs of ground motions are used for analysis, the maximum value of the response parameter of interest shall be used for design. In this study, fast nonlinear analysis (FNA) has been performed for seismic assessment of the bridge. FNA is a nonlinear modal time history analysis method useful for the static or dynamic evaluation of linear or nonlinear structural systems [25]. Because of its computationally efficient formulation, FNA is well-suited for time history analysis, and often recommended over direct-integration applications. This method is primarily linear elastic but has a limited number of predefined nonlinear elements [26]. For this nonlinear modal analysis, all nonlinearity is restricted to the Link elements. The efficiency of FNA method is largely due to the separation of the nonlinear-object force vector  $R_{NL}(t)$  from the elastic stiffness matrix and the damped equations of motion, as seen in the fundamental equilibrium equation of FNA, expressed as Eq. (10):

$$M\ddot{u}(t) + C\dot{u}(t) + Ku(t) + R_{NL}(t) = R(t) \quad (10)$$

Where  $M$ ,  $C$ , and  $K$  are the mass matrix, damping matrix and stiffness matrix, respectively. Time-dependent vectors of  $u(t)$ ,  $\dot{u}(t)$ , and  $\ddot{u}(t)$  are relative displacements, velocities, and accelerations.  $R(t)$  is the external vector of applied loads. Furthermore, the Newton-Raphson iteration procedure

consisting of corrective unbalanced forces is employed within each time step until equilibrium condition is achieved.

## 6. RESULTS AND DISCUSSION

The purpose of this section is to investigate and compare the influence of the LRB and the ERB isolators on the seismic responses of the Hesarak multi-span bridge. The period of vibrations, pier base shear, the isolator's displacement and force, the displacement and bending moment of the piers, the deck acceleration, and the amount of energy dissipations by the isolators have been considered. CSIBridge computing platform is adopted to perform an eigenvalue analysis and nonlinear time history analyses using seven pairs of ground motions in the longitudinal and transverse directions. The results of different cases are extracted, compared, and discussed as follows.

The purpose of seismic isolation is the reduction of forces in the structure and the foundation. In which, one of the solutions is to increase the vibration period of the structure. Increasing the vibration period reduces the structural response according to the design spectrum, which has been investigated in many studies as the effect of structural period transitions. However, increasing the period of the structure reduces the lateral stiffness of the bridge that increases the lateral displacement of the structure. As expected, the isolation system increases the period of the structure in comparison with the non-isolated state. Table 6 indicates that the LRB isolator caused an increase of approximately 6.5 times the fundamental period of vibration for the first mode of the bridge compared to the non-isolated bridge and increased about two times compared to the bridge with the ERB isolator.

Table 6. The fundamental period for the studied bridge (sec)

Non-isolated	With ERB isolator	With LRB isolator
0.42	1.37	2.7

Using the LRB isolator, the pier base shear is sharply decreased both in longitudinal and transverse directions in different earthquake motions, which causes less force to enter the bridge. The reasons for reducing the base shear are the increase in the period and damping of the bridge, which Roy and Dash [3] also refer to it. The intended damping was assumed to be 30% for the isolator of the bridge. The bridge is also analyzed under the 15% damping. The results show that the decrease in damping causes an increase in the pier base shear, the magnitude of increase under the El Centro record in the longitudinal and transverse direction is 12% and 17%, respectively. Under the Cape Mendocino record,

it reaches 18.8% in the longitudinal direction and up to 13.2% in the transverse direction. Table 7 and Fig. 9 show the maximum pier base shear force of the bridge with the ERB and the LRB isolators under given ground motions. Also, the base shear time history results of the bridge due to the three representative earthquake motions of Tabas, Northridge, and Kobe is shown in Fig. 10. It can be seen that the rate of reduction of the base shear in the longitudinal and transverse direction is 80% under the Tabas earthquake, for Northridge earthquake in the longitudinal direction is 82% and in the transverse direction is 87%, and due to the Kobe earthquake in the longitudinal direction is about 75% and in the transverse direction is about 60%. It can be concluded that the bridge response is earthquake-dependent and varies in different earthquake motions.

Table 7. Maximum base shear force in the bridge (ton)

	Earthquake	ERB isolator	LRB isolator
<b>Longitudinal direction</b>	Tabas	3127.00	583.20
	El Centro	3345.00	790.63
	Cape Mendocino	3522.50	1293.9
	Northridge	3770.75	655.25
	Kobe	2085.06	528.15
	Chi Chi	3028.20	592/00
	San Simeon	1919.60	769.78
<b>Transverse direction</b>	Tabas	2381.62	475.63
	El Centro	2105.50	710.62
	Cape Mendocino	3087.00	1121.0
	Northridge	3377.45	413.74
	Kobe	1133.40	462.93
	Chi Chi	2650.00	557.00
	San Simeon	1334.00	738.03

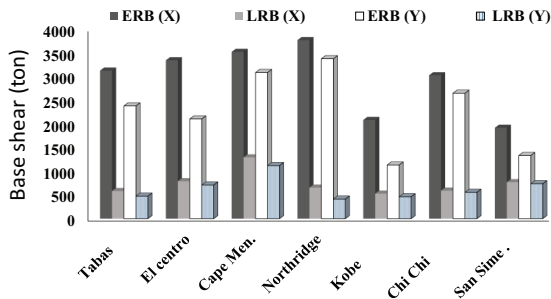


Figure 9. The maximum base shear for the bridge with LRB and ERB due to the given earthquake motions.

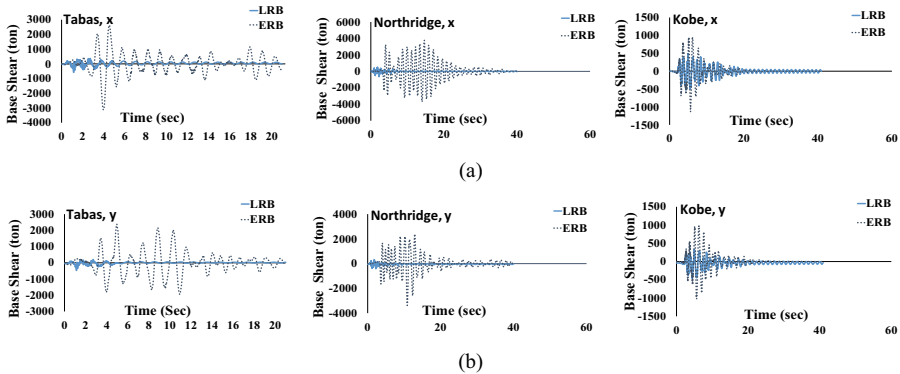


Figure 10. Base shear time history of the bridge due to the three representative earthquake motions: a) Longitudinal direction, and b) Transverse direction.

According to numerical analyses, the LRB isolator reduces the maximum pier bending moment. For instance, the analysis results of the middle pier P4 under various earthquakes are shown in Table 8. As seen, the pier bending moment using the LRB isolator is significantly reduced. For example, this reduction for the Northridge earthquake is 91.5% in the transverse direction and 73.4% in the longitudinal direction. Table 9 presents the pier head relative displacement of P4 column in the longitudinal direction of the bridge. Also, Fig. 11 shows the displacement time history of the middle-end P4 pier head under the three representative earthquake ground motions. As shown, the LRB isolator reduces the pier head displacement against the ERB isolator. Generally, the displacement reduction depends on the earthquake ground motion. According to Table 9, the maximum pier head relative displacement of the bridge reaches: for ERB 28 cm and for LRB 0.3 cm under the El Centro earthquake. It is noted that when bridges are subjected to near-field ground motions, they do not often return to their initial vertical positions and may have considerable residual displacement [27]. In a similar way, Fig. 11 indicates the residual displacement of the bridge model.

Table 8. Reduction of maximum bending moment of P4 column by LRB isolator (ton.m)

	Earthquake	ERB isolator	LRB isolator	Bending moment reduction
<b>Longitudinal direction</b>	Tabas	2064.00	568.17	72.50%
	El Centro	2230.00	663.41	70.20%
	Cape Mendocino	2399.00	913.34	62.00%
	Northridge	2500.00	666.00	73.36%
	Kobe	1385.00	509.50	63.20%
	Chi Chi	3625.00	548.64	85.00%
	San Simeon	1291.00	641.00	50.00%
<b>Transverse direction</b>	Tabas	4427.00	555.00	87.50%
	El Centro	4322.80	1184.40	72.60%
	Cape Mendocino	5157.63	1645.50	68.10%
	Northridge	6146.20	527.16	91.50%
	Kobe	2168.70	818.00	62.00%
	Chi Chi	2021.00	897.32	55.60%
	San Simeon	2622.50	1049.00	60.00%

Table 9. Comparison of P4 pier head relative displacement with ERB and LRB isolator (mm)

Earthquake	ERB isolator	LRB isolator	Displacement reduction
Tabas	8.17	2.25	72.50%
El Centro	277.50	2.82	99.30%
Cape Mendocino	9.50	3.60	62.00%
Northridge	10.00	0.97	90.00%
Kobe	41.60	2.018	95.00%
Chi Chi	8.00	2.17	72.80%
San Simeon	5.11	2.50	51.00%

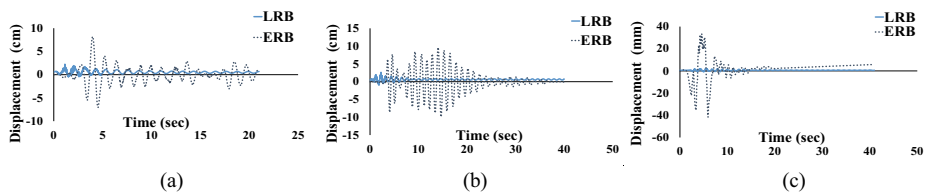


Figure 11. P4 pier head displacement time history of the bridge due to the three representative earthquake motions: a) Tabas, b) Northridge, and c) Kobe.

The maximum absolute deck acceleration of the bridge is shown under given earthquake motions for the ERB and the LRB isolators in Table 10 and Fig. 12. As seen, the advantage of using an LRB isolator is to reduce the acceleration to the deck. As indicated before, the results are corresponding to the isolator with damping ratio  $\zeta=30\%$ . However, the deck acceleration will increase in the case of 15% damping ratio. For example, the maximum deck acceleration of the bridge under the Cape Mendocino earthquake motion for  $\zeta=15\%$  is  $1.8 \text{ m/sec}^2$ , which shows a 28% increase compared to an isolator with

30% damping ratio. Similarly to Vatanshenas et al. [11], the reason for the differences between the deck accelerations is the frequency content of the selected earthquake ground motions. Furthermore, Fig. 13 shows the deck acceleration time histories due to the three representative Tabas, Northridge, and Kobe earthquake ground motions in both longitudinal and transverse directions.

Table 10. The maximum absolute deck acceleration of the bridge (m/sec<sup>2</sup>)

	Earthquake	ERB isolator	LRB isolator
<b>Longitudinal direction</b>	Tabas	4.10	0.67
	El Centro	4.38	1.08
	Cape Mendocino	4.69	1.40
	Northridge	4.86	0.81
	Kobe	2.65	0.68
	Chi Chi	4.10	0.92
	San Simeon	2.62	0.99
	<b>Transverse direction</b>	Tabas	4.80
El Centro		5.29	2.14
Cape Mendocino		7.72	2.25
Northridge		6.70	0.95
Kobe		3.03	1.06
Chi Chi		6.75	0.07
San Simeon		3.40	1.60

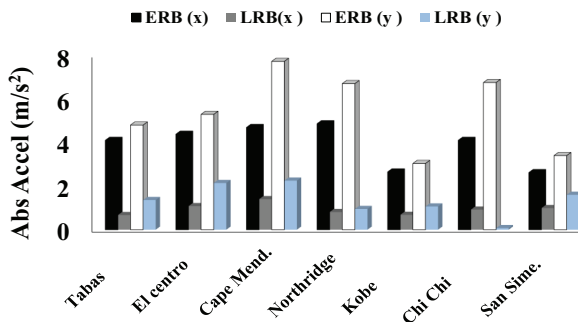


Figure 12. The deck acceleration of the bridge with the LRB and ERB due to the given earthquake motions.

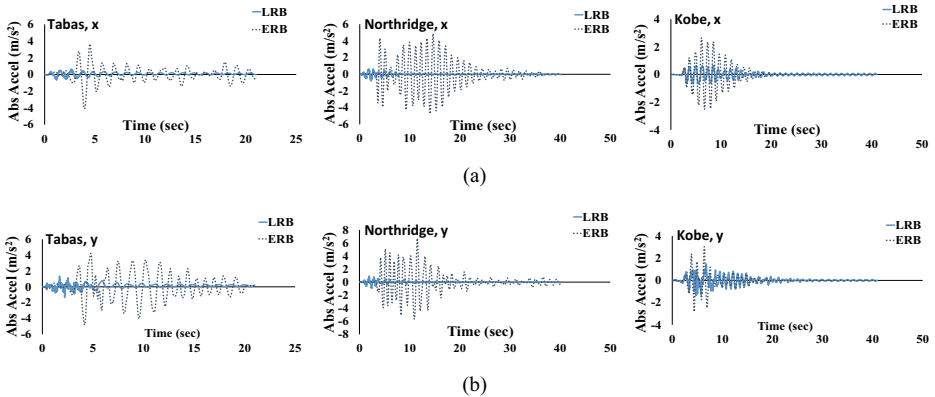


Figure 13. The deck acceleration time history of the bridge due to the three representative earthquake motions: a) Longitudinal direction, and b) Transverse direction.

As shown in Fig. 14, the LRB isolator reduces the input energy of the structure and wastes a high percentage of earthquake input energy, which shows the high separation efficiency. Mendez et al. [10] demonstrate high energy dissipation by the LRB isolator. For the bridge with the ERB isolator, there is no hysterical energy loss due to the lack of the damping and the input energy of the earthquake is dissipated intrinsically. By carefully plotting energy charts and acceleration charts, energy dissipation starts after the maximum acceleration is reached. As shown in Table 11, the maximum amount of earthquake input energy reduction by the LRB isolator is considered to be El Centro earthquake motion, which is 98.5%. The LRB isolator increases the energy dissipation that varies in different earthquakes. However, the isolator of ERB, because of the hysteresis damping, amortize the input energy as inherent damping, which increases the displacement of the ERB isolator to amortize energy, which, in the case of severe earthquakes, does not have the expected performance. The LRB isolator has high energy absorption due to hysterical damping due to the leakage of the lead core and its performance under earthquake motions is well proven.



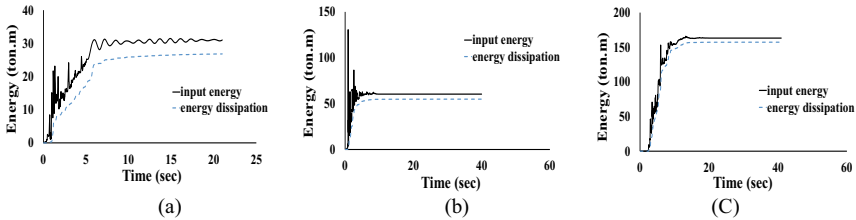


Figure 14. Input and dissipation energy diagrams of the bridge due to the three representative earthquake motions: a) Tabas, b) Northridge, and c) Kobe.

Table 11. The energy dissipation by the LRB isolator (ton.m)

Earthquake	Input energy (ton.m)	Output energy (ton.m)	Energy reduction
Tabas	31.45	26.80	85.00%
El Centro	1141	1124	98.50%
Cape Mendocino	728.0	671.0	92.00%
Northridge	47.50	21.50	45.26%
Kobe	165.7	157.0	94.70%
Chi Chi	377.0	356.0	94.50%
San Simeon	361.0	350.0	97.00%

The hysteresis diagram describes the behavior of the member under earthquake reciprocating loads, which is shown as a load-displacement diagram. If the produced curve has symmetry, it shows the structural behavior is uniform against earthquake. The next feature of the hysteresis loop is the surface area enclosed by the curve, the more the surface area, the greater the energy absorbed by the structure, indicating that the structure is more ductile. Another feature is the number of hysteresis curve cycles, the higher the number of cycles, the later representing the deterioration of the member. Thus, regarding the characteristics of the hysteresis diagram, we can refer to three factors: the number of cycles, the area enclosed by the loop, and the symmetry. According to Fig. 15, the designed LRB has a slender diagram and fewer cycles under the Northridge, Cape Mendocino, and Tabas earthquakes, which represents less damping, thus resulting in less energy absorption and early isolation failure. However, the LRB isolator performance is more suitable for other earthquake motions because their hysteresis loops are stable and have a more area enclosed by the load-displacement diagram. Fig. 16 shows, for instance, the shear force-deformation curve of the ERB due to the Cape Mendocino earthquake motion that does not fit the condition of an appropriate hysteresis loop.

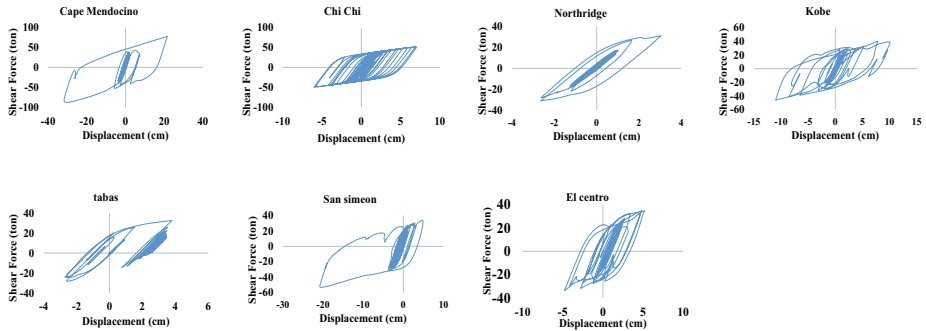


Figure 15. Hysteresis loop for the LRB isolator subjected to the given earthquake motions.

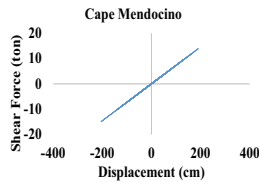


Figure 16. Force-displacement curve for the ERB due to the Cape Mendocino earthquake motion.

## 7. CONCLUDING REMARKS

In this paper, the effects of LRB isolation system on improving the seismic behavior of a multi-span pre-stressed bridge was evaluated and compared with the case of the existing ERB isolator. A 3D FEM of the isolated bridge was developed in CSIBridge. Based on the results of the analyses, the specific conclusions are as follows:

1. The use of an LRB isolator instead of the ERB increased the fundamental period of the bridge by a factor of 2.
2. The base shear of the bridge using the LRB isolator is significantly reduced compared to the ERB. The reduction reached 82.6% and 87.75% in the longitudinal and transverse directions, respectively.
3. The LRB isolator reduced the bending moment by up to 85% compared to the ERB.
4. The absolute deck acceleration of the bridge was significantly reduced using the LRB so that the amount of this reduction is up to 70%.

5. The performance of the LRB isolator was significant in terms of energy dissipation capacity, the input energy reduced up to 94% when LRB system was applied.
6. The LRB performance is suitable for reducing the pier head displacement so that the reduction is up to 62%.

Therefore, one of the main alternatives for the seismic improvement of the Hesarak Bridge is the replacement of the existing ERB isolators with the LRB. It must be noted that the response is ground motion sensitive; hence designers should use a sufficient number of seismic records to carry out the analysis for design.

## **ACKNOWLEDGEMENTS**

The structural and geotechnical data of the Hesarak Bridge provided by the municipality of Karaj city, Iran is gratefully acknowledged. We also thank the anonymous reviewers for their helpful comments on the improvement of the manuscript.

## **REFERENCES**

1. Mason, S.E. "Seismic Isolation-The Gold Standard of Seismic Protection", Structure Magazine, California, pp. 11-14 (2015).
2. Robinson, W.H. "Lead-Rubber Hysteretic Bearing Suitable for Protecting Structures During Earthquakes", Earthquake Engineering and Structural Dynamics, Vol. 10, No. 4, pp. 593-604 (1982).
3. Roy, S.S., Dash, S.R. "Dynamic Behavior of the Multi Span Continuous Girder Bridge with Isolation Bearings", International Journal of Bridge Engineering (IJBE), Vol. 6, No. 2, pp. 01-23 (2018).
4. Code No. 523 "Guideline for Design and Practice of Base Isolation Systems in Buildings," Vice Presidency for Strategic Planning and Supervision, Tehran, Iran (2010).
5. Naiem, F., Kelly, J.M. "Design of Seismic Isolated Structures: From Theory to Practice," John Wiley and Sons, Inc. New York, USA (1999).
6. Turkington, D. H., Carr, A. J., Cooke, N., and Moss, P. J. "Seismic Design of Bridges on Lead-Rubber Bearings," Journal of Structural Engineering, ASCE, Vol. 115, No. 12 pp. 3000-3016 (1989).
7. Zahraei, M., Sami, H. "Seismic Performance Evaluation of Bridges with Existing Expansion Bearings," Journal of Transportation Research, Vol. 5, No. 4, pp. 319-331 (2009).
8. Asif, H., Min-Se K., Thang Dai, D., and Jin-Hoon J. "Effect of Lead Rubber Bearing Characteristics on the Response of Seismic-Isolated Bridges", KSCE Journal of Civil Engineering, Vol. 12, No. 3, pp. 187-196 (2008).
9. Tubaldi, E., Mitoulis, S., Ahmadi, A., Muh, H. A. "A parametric study on the axial behavior of elastomeric isolators in multi-span Bridges subjected to horizontal seismic excitations", Bull Earthquake Eng, Vol. 14, No. 4, pp. 1285-1310 (2016).

10. Mendez Galindo, C., Spuler, T., Moor, G., Stirnimann, F. "Design, Full-scale Testing, and CE Certification of Anti-Seismic Devices According to the New European Standard EN 15129: Elastomeric Isolators", 15<sup>th</sup> World Conference on Earthquake Engineering, Lisbon, Portugal (2012)
11. Vatanshen, A., Sharif Bajestany, D., Aghelfard, A. "The Effect of Seismic Isolation on the Response of Bridges," International Journal of Bridge Engineering (IJBE), Vol. 6, No. 3, pp. 61-74 (2018).
12. Park, K. S., Jung, J. H., Lee, L.W. "A comparative study of A seismic performances of base isolation systems for multi-span continuous bridge", Engineering Structures, Vol. 24, No. 8, pp. 1001-1013 (2002).
13. Chauhan, K.M., Shah, B.J. "Excel spreadsheet for Design of Lead Rubber Bearings for Seismic Isolation of Bridge", International Journal of Advanced Engineering Research and Studies, Vol. 2, No. 3, pp. 60-62 (2013).
14. Edalati A.A. "Investigating the performance of seismic isolation systems in improving the behavior of urban bridges under Earthquake (A case study on the Hesarak Bridge)," MSc Thesis, University of Kashan, Iran (2019).
15. <http://www.google.Earth/.html>
16. Municipality of Karaj "Report of the studies of Hesarak Bridge," University of Science and Technology, Tehran, Iran (2015) (in Persian).
17. BHRC. "Iranian code of practice for seismic resistant design of buildings (Standard No. 2800)," 4<sup>th</sup> Edition, Building and Housing Research Center, Tehran, Iran (2014).
18. Tahghighi, H. "Simulation of Strong Ground Motion using the Stochastic Method: Application and Validation for Near-Fault Region," Journal of Earthquake Engineering, Vol. 16, pp. 1230-1247 (2012).
19. Tahghighi, H., Rabiee, M. "Influence of Foundation Flexibility on the Seismic Response of Low-to-Mid-Rise Moment Resisting Frame Buildings," International Journal of Science and Technology, SCIENTIA IRANICA, A, Vol. 24, No. 3, pp. 979-992 (2017).
20. CSIBridge "Integrate Finite Element Analysis and Design of Bridges," User manual, Ver. 19.2, Berkley, California, USA (2017).
21. AASHTO "Guide Specifications for Seismic Isolation Design," 4<sup>th</sup> Ed., American Association of State Highway and Transportation Officials, Washington DC, USA (2014).
22. Park, Y. J., Reinhorn, A. M., Kunnath, S. K. "IDARC: Inelastic damage analysis of reinforced concrete frame-shear-wall structures," Tech. Rep. NCEER-87-0008, State University of New York at Buffalo, Buffalo, NY, USA (1987).
23. PEER. "Pacific Earthquake Engineering Research center strong motion database," <http://peer.berkeley.edu> (2018).
24. ASCE. "Minimum Design Loads for Buildings and Other Structures (ASCE/SEI 7-10)," American Society of Civil Engineers/Structural Engineering Institute, Reston, VA, USA (2010).
25. <https://wiki.csiamerica.com>
26. Lee, H.H., Hur, M.W., Jiang, H., You, Y.C., Kim, K.H. "Evaluation of Dynamic Characteristics of Base Isolated Residential Building," 14<sup>th</sup> World Conference on Earthquake Engineering, Beijing, China (2008).
27. Ansari, M., Daneshjoo, F., Soltani, M. "A New Combinational Force-Displacement Hysteresis Model Presented to Estimate Seismic Residual Displacement in Single-Column Concrete Bridges," Journal of Transportation Engineering, Vol. 7, No. 2, pp. 223-236 (2015).

## LIST OF TABLES AND FIGURES

Table 1. Specifications of the bridge

Table 2. ERB isolator specifications used in the bridge

Table 3. Material properties of rubber used in LRB design

Table 4. LRB isolator specifications

Table 5. Specifications of the accelerograms used in the analysis [23]

Table 6. The fundamental period for the studied bridge (sec)

Table 7. Maximum base shear force in the bridge (ton)

Table 8. Reduction of maximum bending moment of P4 column by LRB isolator (ton.m)

Table 9. Comparison of P4 pier head relative displacement with ERB and LRB isolator (mm)

Table 10. The maximum absolute deck acceleration of the bridge (m/sec<sup>2</sup>)

Table 11. The energy dissipation by the LRB isolator (ton.m)

Figure 1. Aerial photo of the Hesarak Bridge [15].

Figure 2. General view of the Hesarak Bridge.

Figure 3. Cross-section through the deck of Hesarak Bridge (uint in cm) [16].

Figure 4. Details of the Hesarak Bridge (uint in cm): a) Abutment, and b) Pier section [16].

Figure 5. Longitudinal profile of the bridge [16].

Figure 6. 3D finite element model of the bridge.

Figure 7. LRB isolator system (after [13]).

Figure 8. Force-displacement model for LRB: a) Shear behavior, and b) Axial behavior.

Figure 9. The maximum base shear for the bridge with LRB and ERB due to the given earthquake motions.

Figure 10. Base shear time history of the bridge due to the three representative earthquake motions: a) Longitudinal direction, and b) Transverse direction.

Figure 11. P4 pier head displacement time history of the bridge due to the three representative earthquake motions: a) Tabas, b) Northridge, and c) Kobe.

Figure 12. The deck acceleration of the bridge with the LRB and ERB due to the given earthquake motions.

Figure 13. The deck acceleration time history of the bridge due to the three representative earthquake motions: a) Longitudinal direction, and b) Transverse direction.

Figure 14. Input and dissipation energy diagrams of the bridge due to the three representative earthquake motions: a) Tabas, b) Northridge, and c) Kobe.

Figure 15. Hysteresis loop for the LRB isolator subjected to the given earthquake motions.

Figure 16. Force-displacement curve for the ERB due to the Cape Mendocino earthquake motion.

*Received 30.06.2019, Revised 15.09.2019*